

Acute inhibition of transient receptor potential vanilloid-type 4 cation channel halts cytoskeletal dynamism in microglia

Peer-reviewed author version

BEEKEN, Jolien; MERTENS, Melanie; Stas, Nathan; KESSELS, Sofie; AERTS, Liese; JANSSEN, Bieke; Mussen, Femke; Pinto, Silvia; Vennekens, Rudi; RIGO, Jean-Michel; Nguyen, Laurent; BRONE, Bert & AGUIAR ALPIZAR, Yeranddy (2022) Acute inhibition of transient receptor potential vanilloid-type 4 cation channel halts cytoskeletal dynamism in microglia. In: GLIA (New York, N.Y. : Print), 70 (11) , p. 2157-2168.

DOI: 10.1002/glia.24243

Handle: <http://hdl.handle.net/1942/37951>

1 **Acute inhibition of transient receptor potential vanilloid-type 4 cation channel halts**  
2 **cytoskeletal dynamism in microglia**

3 Running title: TRPV4 inhibition hinders microglial dynamism

4 Jolien Beeken<sup>1,2</sup>, Melanie Mertens<sup>1</sup>, Nathan Stas<sup>1</sup>, Sofie Kessels<sup>1</sup>, Liese Aerts<sup>1</sup>, Bieke Janssen<sup>1</sup>,  
5 Femke Mussen<sup>1</sup>, Silvia Pinto<sup>3</sup>, Rudi Vennekens<sup>3</sup>, Jean-Michel Rigo<sup>1</sup>, Laurent Nguyen<sup>2</sup>, Bert Brône<sup>1†</sup>,  
6 Yeranddy A. Alpizar<sup>1†</sup>

7

8 <sup>1</sup> Hasselt University, BIOMED, Diepenbeek, Belgium

9 <sup>2</sup> Université de Liège, GIGA-Stem-Cells, Liège, Belgium

10 <sup>3</sup> Laboratory for Ion Channel Research, VIB-KU Leuven, Leuven, Belgium

11 † These authors contributed equally to this work as co-senior authors

12

13 Correspondence to:

14 Yeranddy A. Alpizar email: yeranddy.aguiaralpizar@uhasselt.be

15 Bert Brône email: bert.brone@uhasselt.be

16 **ACKNOWLEDGEMENTS**

17 We thank Melissa Jans and Yennick Geuens for the maintenance of the mouse colonies at BIOMED;  
18 Rosette Beenaerts and Petra Bex for their technical assistance with genotyping and cell culture  
19 maintenance; and Dr. Sam Duwé from the Advanced Optical Microscopy Centre for training, support  
20 and access to the instrumentation. The graphical abstract was created in BioRender.com.

21 J.B. is a PhD student supported by the Special Research Foundation (BOF17DOCLI01) from Hasselt  
22 University and Université de Liège. M.M. is a PhD student supported by the Special Research  
23 Foundation UHasselt (BOF21DOC21). Y.A.A is supported by an FWO senior postdoctoral fellowship  
24 (12H8220N). This work was supported by FWO research grants (1521619N), Special Research  
25 Foundation UHasselt (BOF16NI04, BOF20KP11, BOF21KP06, BOF21GP05), Sint Gillis autism  
26 research grant, the ROTARY Espoir en Tête – Hoofdzaak er is Hoop, the F.R.S.-F.N.R.S. (Synet; EOS  
27 0019118F-RG36), the Fonds Leon Fredericq, the Fondation Médicale Reine Elisabeth, the Fondation  
28 Simone et Pierre Clerdent, the Belgian Science Policy (IAP-VII network P7/20), and the ERANET  
29 Neuron STEM-MCD and NeuroTalk.

30 **AUTHOR CONTRIBUTIONS**

31 B.B. and Y.A.A conceived and designed the project. J.B., M.M., S.K. and Y.A.A. designed or conducted  
32 the *ex vivo* branch motility experiments. J.B., M.M. and Y.A.A. conducted microglial morphology and  
33 density experiments. J.B., L.A. and Y.A.A. performed and quantified the *in vitro* random walk. J.B.,  
34 N.S., B.J., F.M. and Y.A.A. isolated and cultured primary microglia and conducted the *in vitro*  
35 morphology and motility experiments. J.B. contributed with the analysis of all experiments. N.S.,  
36 J.B., M.M. and Y.A.A. conducted and quantified the tubulin and filopodia imaging experiments. S.P.  
37 and R.V. provided the *Trpv4* KO mice. All authors contributed to the interpretation of data. J.B. and  
38 Y.A.A. wrote the manuscript with input from all co-authors.

39 **CONFLICT OF INTEREST**

40 The authors declare no competing interests.

41 **Word count (total):** 5118

42 **ABSTRACT (Word count: 193)**

43 Microglia, the resident macrophages of the central nervous system are highly motile cells that  
44 support brain development, provision neuronal signaling and protect brain cells against damage.  
45 Proper microglial functioning requires constant cell movement and morphological changes.  
46 Interestingly, the transient receptor potential vanilloid 4 (TRPV4) channel, a calcium-permeable  
47 channel, is involved in hypoosmotic morphological changes of retinal microglia and regulates  
48 temperature-dependent movement of microglia cells both *in vitro* and *in vivo*. Despite the broad  
49 functions of TRPV4 and the recent findings stating a role for TRPV4 in microglial movement, little is  
50 known about how TRPV4 modulates cytoskeletal remodeling to promote changes of microglial  
51 motility. Here we show that acute inhibition of TRPV4, but not its constitutive absence in the *Trpv4*  
52 KO cells, affects the morphology and motility of microglia *in vitro*. Using high-end confocal imaging  
53 techniques, we show a decrease in actin-rich filopodia and tubulin dynamics upon acute inhibition of  
54 TRPV4 *in vitro*. Furthermore, using acute brain slices we demonstrate that *Trpv4* knockout microglia  
55 display lower ramification complexity, slower process extension speed and consequently smaller  
56 surveyed area. We conclude that TRPV4 inhibition triggers shifts in cytoskeleton remodelling of  
57 microglia influencing their migration and morphology.

58

59 **KEYWORDS**

60 Microglia, TRPV4, Cytoskeleton, Morphology, Random persistent walk, Process motility

61

62 **MAIN POINTS**

- 63 - Acute inhibition of TRPV4 abrogates microtubule and actin-rich filopodia dynamism in  
64 microglia *in vitro*.  
65 - *Trpv4* KO microglia exhibit less ramification complexity and slower process extension  
66 speed *in situ*.

67

68 **DATA AVAILABILITY STATEMENT**

69 Data available on request from the authors.

70

71

72 **1. INTRODUCTION (Word count: 699)**

73 Microglia, the resident immune cells of the central nervous system (CNS), play an essential role  
74 during development and homeostasis (Smolders *et al.*, 2019; Wolf *et al.*, 2017). They mediate brain  
75 homeostasis by maintaining neuronal networks, stimulating tissue repair as well as eliminating dead  
76 or damaged cells, intruding pathogens and redundant synapses via phagocytosis (Colonna &  
77 Butovsky, 2017; Salter & Stevens, 2017; Wolf *et al.*, 2017). For proper functioning, microglia require  
78 constant movement either through process motility or migration, events that are highly dependent  
79 on cytoskeletal rearrangements (Nimmerjahn *et al.*, 2005; Wolf *et al.*, 2017). It has been widely  
80 established that cytoskeleton remodeling is induced through a molecular machinery consisting of  
81 membrane receptors (e.g., ion channels, integrins) which allow the cell to sense environmental  
82 changes, hereby regulating cell responses (Franco-Bocanegra *et al.*, 2019; Madry & Attwell, 2015;  
83 Nimmerjahn *et al.*, 2005; Ohsawa & Kohsaka, 2011). Although several ion channels have been  
84 shown to mediate protrusion formation and migration in microglia (Hines *et al.*, 2009; Smolders *et*  
85 *al.*, 2019; Swiatkowski *et al.*, 2016), the molecular signaling pathways underpinning cytoskeleton  
86 remodeling in microglia remain largely unknown.

87 Recent *in vivo* research showed that microglial processes mainly exhibit Ca<sup>2+</sup> signaling in their  
88 protruding branches without significant fluctuations in somatic Ca<sup>2+</sup> levels (Umpierre *et al.*, 2020).  
89 Noteworthy, local Ca<sup>2+</sup> increases necessary for cell dynamics and movement are not solely initiated  
90 by chemoattractant signal transduction but also by stretch-activated calcium-permeable channels  
91 from the transient receptor potential (TRP) channel family (Wei *et al.*, 2009).

92 TRP channels are involved in a variety of physiological processes such as nociception, proprioception  
93 and thermosensation (Canales *et al.*, 2019; Liu & Montell, 2015; Nilius & Owsianik, 2011). They  
94 have a key function in cellular processes such as volume regulation, proliferation, activation and cell  
95 death (Becker *et al.*, 2005; Clapham, 2003; Echeverry *et al.*, 2016; Ryskamp *et al.*, 2016). Several  
96 Ca<sup>2+</sup>-permeable TRP channels are expressed in microglial cells and have been reported to play a  
97 pivotal role in regulating their function (Chakraborty & Goswami, 2022; Echeverry *et al.*, 2016;  
98 Konno *et al.*, 2012; Mizoguchi *et al.*, 2014; Nishimoto *et al.*, 2021; Sappington & Calkins, 2008; Sun  
99 *et al.*, 2014). For example, TRPV1 is mainly associated with neurotoxicity as it is involved in the  
100 release of proinflammatory cytokines by microglia (Echeverry *et al.*, 2016). On the other hand,  
101 TRPM2 is essential for the temperature-dependent movement of microglia as well as stress-induced  
102 activation (Echeverry *et al.*, 2016; Nishimoto *et al.*, 2021), while TRPC3 contributes to microglial  
103 activation through the suppression of brain-derived neurotrophic factor (BDNF) (Mizoguchi *et al.*,  
104 2014). More recently, TRPV4 has been implicated in the regulation of microglial morphology and  
105 intracellular signaling in response to hypoosmotic conditions (Redmon *et al.*, 2021) and  
106 temperature-dependent motility (Nishimoto *et al.*, 2021). However, the role of TRPV4 in cytoskeletal  
107 regulation aiding microglial motility remains elusive. Interestingly, TRPV4 is involved in regulating  
108 cytoskeleton rearrangements in endometrial cancer cells by mediating Ca<sup>2+</sup>-influxes (Li *et al.*, 2020).  
109 In neurons a direct interaction of TRPV4 is shown with actin, tubulin and neurofilament proteins  
110 through its C-terminus. The receptor colocalized with actin-rich structures such as filopodia,  
111 lamellipodia and focal adhesion points, thereby regulating cell morphology and net movement of  
112 neurites (Goswami *et al.*, 2010). In astrocytes, TRPV4 influences intracellular pathways involved in  
113 the astrocytic end-feet while in endothelial cells, the cytoskeleton regulates Ca<sup>2+</sup>-influx through

114 TRPV4 (Kanju & Liedtke, 2016). TRPV4 is involved in macrophage phagocytosis and foam cell  
115 formation, two processes highly dependent on Ca<sup>2+</sup>-signaling (Dutta *et al.*, 2020; Michalick &  
116 Kuebler, 2020). It should be noted that TRPV4 activity can be modified by alterations in cell swelling,  
117 stretch, shear flow, plasma membrane phospholipids or the actin cytoskeleton (Canales Coutino &  
118 Mayor, 2021; Liu & Montell, 2015), hereby it is likely that the channel regulates cell motility through  
119 Ca<sup>2+</sup>-mediated mechanotransduction. Here, we assessed the effects of acute TRPV4 inhibition on  
120 microglial morphology, movement and cytoskeleton dynamics. We found that acutely-inhibiting  
121 TRPV4 increases circularity of primary cultured microglia while it decreases area and total  
122 displacement. Furthermore, we showed that cytoskeletal dynamics are decreased upon inhibition of  
123 TRPV4 *in vitro*. Even though constitutive absence of TRPV4 did not alter morphology *in vitro*, we  
124 found significant decreases in morphological complexity and brain surveillance *in situ*.  
125

## 126 **2. MATERIALS AND METHODS (Word count: 1818)**

### 127 **2.1 Animals**

128 All animal experiments were conducted in accordance with the European Community guiding  
129 principles on the care and use of animals and with the approval of the Ethical Committee on Animal  
130 Research of Hasselt University. Animals were group-housed in a temperature and humidity-  
131 controlled room with *ad libitum* access to food and water and a 12 h light-dark cycle. CX3CR1<sup>eGFP/+</sup>  
132 *Trpv4* knockout (KO) and CX3CR1<sup>eGFP/+</sup> wild type (WT) littermates used in this study were obtained  
133 by breeding heterozygous *Trpv4* (*Trpv4*<sup>+/-</sup>) with CX3CR1<sup>eGFP/eGFP</sup> *Trpv4*<sup>+/-</sup> mice. *Trpv4* KO mice were  
134 kindly provided by the Laboratory for Ion Channel Research at KU Leuven. CX3CR1<sup>eGFP/eGFP</sup> (Jung *et*  
135 *al.*, 2000) mice were obtained from the European Mouse Mutant Archive (EMMA) Institute with the  
136 approval of Steffen Jung (Weizmann Institute of Science). For all experiments, mice of either sex  
137 were age-matched and combined with littermate controls.

138

### 139 **2.2 Primary microglia isolation**

140 Cortical microglia from CX3CR1<sup>eGFP/+</sup>WT and CX3CR1<sup>eGFP/+</sup>*Trpv4* KO mice were isolated following  
141 experimental procedures described elsewhere (Stark *et al.*, 2018). In brief, brains of postnatal day  
142 21 (P21) mice were dissected and the midbrain, cerebellum and meninges were carefully removed.  
143 The remainder of the brain was disintegrated in Dulbecco's Modified Eagle's Medium (DMEM, Sigma-  
144 Aldrich, Overijse, Belgium) supplemented with 1% penicillin/streptomycin (P/S, Invitrogen,  
145 Merelbeke, Belgium), followed by incubation with papain (17 U/mg, Sigma-Aldrich) and DNase I (10  
146 mg/ml, Roche, Brussel, Belgium) for 30 min at 37 °C. Cell suspensions were filtered through a 70  
147 µm cell strainer, centrifuged (5 min, 500 x g) and pellets were resuspended in DMEM containing  
148 30% stock isotonic Percoll (SIP, GE Healthcare, Diegem, Belgium). Hereafter, a density gradient was  
149 created by the addition of 70% SIP diluted in PBS and the suspension was centrifuged for 25 min at  
150 650 x g (brake 0, acceleration 4). The cell cloud at the interphase between 30% and 70% was  
151 collected, diluted in 10 ml cold PBS and centrifuged for 10 min at 500 x g. Cell pellets were  
152 resuspended in magnetic-activated cell sorting (MACS) buffer (2 mM EDTA and 0.5% fetal calf serum  
153 (FCS)) and microglia were isolated by positive selection using CD11b microbeads (Miltenyi Biotec,  
154 Gladbach, Germany), following the manufacturer's instructions. CD11b<sup>+</sup> cells were resuspended in  
155 DMEM supplemented with 10% FCS, 10% horse serum (ThermoFisher, Waltham, MA, US) and 1%  
156 P/S (DMEM 10:10:1) and seeded onto glass coverslips (30 x 10<sup>3</sup> cells/well), 24-well plates (30 x 10<sup>3</sup>  
157 cells/well), or 35 mm MatTek glass bottom dishes (10<sup>5</sup> cells/dish, MatTek, Ashland, MA, US) pre-  
158 coated with poly-D-lysine (PDL, 20 µg/ml, Gibco, Waltham, MA, US) and collagen type IV (2 µg/ml,  
159 Sigma-Aldrich), and incubated in a humidified incubator at 37 °C, 8.5% CO<sub>2</sub> for 7 days. Afterwards,  
160 a dynamic ramified morphology was induced by the addition of serum-free medium (hereafter, TIC  
161 medium (Bohlen *et al.*, 2017)) containing 5 µg/ml insulin, 5 µg/ml N-acetyl-cysteine, 100 µg/ml  
162 apo-transferrin, 0.1 µg/ml Na<sub>2</sub>SeO<sub>3</sub>, 1 µg/ml heparan sulfate, 2 µg/ml human TGF-β2 (PeproTech,  
163 Rocky Hill, NJ, US), 0.1 µg/ml murine IL-34 (BioLegend, Amsterdam, The Netherlands), 1.5 µg/ml  
164 ovine wool cholesterol, 3 µg/ml L-glutamine in DMEM/F12. For all experiments, cells were seeded 7  
165 days in DMEM 10:10:1 medium followed by 3-7 days TIC medium unless stated otherwise.

166 For quantification of microglial morphology *in vitro*, images were processed using Fiji software  
167 (Schindelin *et al.*, 2012) by manually defining cell contours and quantifying area and perimeter.  
168 Circularity was calculated as  $4\pi \frac{Area}{Perimeter^2}$ , where a value of 1 indicates a perfect circle.

169

### 170 **2.3 Live-cell tubulin imaging**

171 CD11b<sup>+</sup> cells cultured in 24-well glass bottom plates (Ibidi, Gräfelfing, Germany) (30 x 10<sup>3</sup> cells) or  
172 glass bottom dishes (10<sup>4</sup> cells) were incubated with SiR-Tubulin (1 μM, 45 min, Spirochrome,  
173 Thurgau, Switzerland) at 37 °C. Afterwards, cells were rinsed and imaged before and after being  
174 exposed to solutions containing GSK2193874 (10 μM) or GSK1016790A (300 nM, Tocris Bioscience,  
175 Bristol, United Kingdom) prepared in Krebs (in mM: 150 NaCl, 6 KCl, 10 HEPES, 10 glucose, 1.5  
176 CaCl<sub>2</sub>, 1 MgCl<sub>2</sub>, pH 7.4) either manually or via perfusion by gravity using a multi-barrelled pipette  
177 tip. Live cell tubulin images were obtained using the 100X oil objective followed by structured  
178 illumination microscopy processing on the Zeiss Elyra PS1 and analyzed using the PIVlab toolbox  
179 (Thielicke & Stamhuis, 2014) in MATLAB release 2021a (9.10.0.1649659). For analysis, contrast  
180 was enhanced using a contrast-limited adaptive histogram equalization (set at 20 px) and denoised  
181 (set at 3 px) using pre-processing built-in options. Particle displacements were quantified using a  
182 FFT window deformation algorithm in interrogation areas of 32 pixels (pass 1) and 16 pixels (pass  
183 2). Velocity vectors were filtered to exclude low contrast areas and heat maps representing velocity  
184 magnitudes were generated to include all values of the control condition.

185

### 186 **2.4 Filopodia motility**

187 CD11b<sup>+</sup> cells were cultured in a 24-well glass bottom plate (3 x 10<sup>4</sup> cells/well) and imaged during a  
188 time series before and after exposure to a GSK2193874 (10 μM) solution prepared in Krebs. Confocal  
189 images were obtained using the optimal pinhole size for the 63X oil objective on the Zeiss LSM880-  
190 Airyscan. All images were processed using Fiji software. For analysis and quantification of filopodia  
191 motility, each slice of every stack was filtered (median = 2), thresholded and binarized. To visualize  
192 filopodia, a region of interest in between main processes (ROImp) was manually drawn and data  
193 outside this region was erased. Maximum intensity projections were performed and cumulative  
194 filopodia positions (surveyed area) were calculated as the area of maximum intensity pixels within  
195 the ROImp. For quantification of filopodia length, each filopodium was manually tracked using the  
196 segmented line tool.

197

### 198 **2.5 Persistent random walk**

199 CD11b<sup>+</sup> cells were cultured in DMEM 10:10:1 medium on pre-coated coverslips (30 x 10<sup>3</sup> cells) as  
200 described before. After 5 days in culture, cells were imaged every 15 min for a total duration of 24  
201 h using an Incucyte S3 (Essen BioScience, Newark, United Kingdom). Persistent random walk and  
202 mobility analysis were assessed using Fiji software. Microglial migration, defined as displacement of  
203 the cell body, was manually tracked in 2D for 6 h using the MTrackJ plugin (Meijering *et al.*, 2012)  
204 while the percentage of motile cells was calculated by manually counting the total number cells with  
205 at least one soma displacement event > 10 μm over 10 h.

206

207

## 208 **2.6 Brain perfusion, immunofluorescence and imaging**

209 Wild type CX3CR1<sup>eGFP/+</sup> and CX3CR1<sup>eGFP/+</sup> *Trpv4* KO mice were anesthetized at P21 by intraperitoneal  
210 injection of 2.5 mg/g (body weight) of Dolethal. Mice were transcardially perfused with cold PBS  
211 containing heparin (20 I.U.; Heparine LEO 5.000 I.U./ml, Lier, Belgium) followed by 4% cold  
212 paraformaldehyde (PFA). Brains were dissected and incubated in 4% PFA overnight at 4 °C, washed  
213 with PBS and kept in PBS-azide (0.01%) until slicing. Free-floating sections (100 µm) were cut using  
214 a Microm HM650V Vibratome (Prosan, Monheim, Germany) and stained with DAPI (Sigma-Aldrich)  
215 for 15 min. The sections were mounted on microscope slides (ThermoScientific) and coverslipped in  
216 fluorescent mounting medium (Immu-Mount, ThermoScientific). To investigate morphology or  
217 volumetric density, cortical sections were imaged using a confocal microscope (Zeiss LSM880) and  
218 eGFP<sup>+</sup> microglia were visualized using the Argon 488 nm laser. Microglial cells were captured within  
219 a 20 µm z-stack, stepping 1 µm using a 63X oil objective (NA 1.4). For surface density analysis,  
220 cortical brain sections were imaged using an automated slide scanner (Zeiss AxioScan.Z1) with 20X  
221 objective.

222

## 223 **2.7 Sholl and density analysis**

224 Microglial morphology was assessed by Sholl analysis, as described by Kyrargyri *et al.* (Kyrargyri *et al.*  
225 *et al.*, 2020). In brief, cell reconstructions were performed using 3D automatic cell tracing in Vaa3D  
226 software (<http://www.vaa3D.org>) using the APP2 (All-path-pruning 2.0) algorithm to generate 3D  
227 skeletons of the ramified microglia (Xiao & Peng, 2013). The morphological features were analyzed  
228 using a length-based hierarchical pruning method, as previously described by (Kyrargyri *et al.*,  
229 2020). Custom codes in MATLAB are available at <https://github.com/AttwellLab/Microglia>. Microglial  
230 density was quantified in the secondary motor cortex layer 1, 2/3 and 5 by calculating the number  
231 of cells per area unit (mm<sup>2</sup>). Analyses were carried out with experimenters blinded to the genotype.

232

## 233 **2.8 Two-photon imaging of acute brain slices**

234 P21 mice were sacrificed by decapitation followed by quick brain dissection in oxygenated ice-cold  
235 slicing solution containing (in mM): 120 N-methyl-d-glucamine, 2.5 KCl, 25 NaHCO<sub>3</sub>, 1 CaCl<sub>2</sub>, 7  
236 MgCl<sub>2</sub>, 1.2 NaH<sub>2</sub>PO<sub>4</sub>, 20 D-glucose, 2.4 Na<sup>+</sup> pyruvate, 1.3 Na<sup>+</sup>-L-ascorbate, pH 7.3-7.4, ~ 300 mOsm.  
237 Brains were coronally sliced (300 µm-thick) using a vibratome (LEICA VT1200S) and allowed to  
238 recover for 1 h at 36 °C in oxygenated artificial CSF (aCSF) containing (in mM): 126 NaCl, 2.5 KCl,  
239 26 NaHCO<sub>3</sub>, 2 CaCl<sub>2</sub>, 2 MgCl<sub>2</sub>, 1.25 NaH<sub>2</sub>PO<sub>4</sub>, 10 D-glucose, pH 7.3-7.4, ~ 300 mOsm. Experiments  
240 were performed under continuous perfusion of oxygenated (95% O<sub>2</sub> and 5% CO<sub>2</sub>) aCSF at room  
241 temperature to preserve slice health.

242 Acute brain slice imaging was performed using a Zeiss LSM880-Airyscan confocal microscope (with  
243 a 40X EC plan-Neofluar objective, NA 1.4) provided with a Mai Tai DeepSee Ti:Sapphire-pulsed laser  
244 (Spectra-Physics, Utrecht, The Netherlands) tuned at 920 nm (13 mW intensity, 1.54 µs pixel dwell).  
245 Stacks were recorded starting from a minimal depth of 50 µm above the surface of the slice to avoid  
246 cells being activated by slicing (Eyo *et al.*, 2014; Schiefer *et al.*, 1999).

247 For branch motility analysis, a z-stack spanning 14 µm with serial optical sections every 1 µm was  
248 acquired every minute during 10 min.

249



250 **2.9 Acute brain slice image processing**

251 All images were processed as described before (Bernier *et al.*, 2019; Kyrargyri *et al.*, 2020) using  
252 Fiji software. For analysis and quantification of microglial surveillance, each slice of every stack was  
253 filtered (median filter = 1) followed by subtraction of background with a ball size of 30. The 3D-  
254 stacks were then registered for drifting by applying the StackReg plugin with rigid body  
255 transformation (Thevenaz *et al.*, 1998). Maximum intensity projections were performed and  
256 individual cells were selected by manually drawing a region of interest and erasing data outside this  
257 region. These individual cells were then manually binarized by applying Huang threshold which is  
258 based on the intensity and morphology of the cell. Threshold values were set ensuring the presence  
259 of all microglial processes in all the different frames. To quantify surveillance, for each movie,  
260 consecutive binarized images were pairwise subtracted to generate a new movie consisting of pixels  
261 that represent moving processes. Surveyed area was then calculated as the sum of these pixels over  
262 a time span of 10 min. Extension and retraction speed of microglial processes were calculated by  
263 tracking individual branches using the MTrackJ plugin (Meijering *et al.*, 2012) for a total duration of  
264 10 min.

265

266 **2.10 Statistical analysis**

267 Statistical analysis and graphs were produced using Prism 9 (GraphPad Software) and OriginPro  
268 9.0.0 (OriginLab, Northampton, MA, US). Data distributions were assessed for normality (Shapiro-  
269 Wilk) and parametric or non-parametric two-tailed tests were applied accordingly. The reader is  
270 referred to the figure legends for details about the sample size and specific statistical analysis. Box  
271 graphs represent median (middle line) and SD (box length). Individual data points are shown in light  
272 gray. *P* values smaller than 0.05 were considered significant.

273

274 **3. RESULTS (Word count: 1448)**

275 **3.1 TRPV4 regulates microglial morphology and motility *in vitro***

276 First, we sought to determine the contribution of basal TRPV4 activity in the regulation of microglial  
277 morphology *in vitro*. To recapitulate the phenotype of microglial cells *in vivo*, we used a combination  
278 of survival-promoting cues (TGF- $\beta$ 2, IL-34, and cholesterol) in serum-free medium (TIC medium  
279 (Bohlen *et al.*, 2017)). Under this condition, cultured microglia from wild type (WT) animals are  
280 highly ramified, exhibiting a small cell body and long thin processes with filopodia (**Figure 1a**,  
281 **Figure 3a**). We assessed the morphological differences with cultured microglia from *Trpv4* knockout  
282 (KO) mice by quantifying cell shape (circularity) and size (area). Interestingly, the morphological  
283 complexity of microglia remained unchanged in cells with a constitutive deficiency of TRPV4 (*Trpv4*  
284 KO), with cells equally abundant in ramifications (low circularity values) and similar cellular area  
285 (**Figure 1a, b**).

286 Next, we examined the effect of acute inhibition of TRPV4 activity on microglial morphology. For  
287 this, we analyzed the morphological features using live-cell imaging on WT primary microglia treated  
288 with different concentrations of three TRPV4 antagonists, namely GSK2193874 (hereafter GSK21),  
289 HC067047 (HC) and RN9893 (RN). Whereas vehicle (0.2% DMSO)-treated microglia remained highly  
290 ramified and motile over time (up to 48 hours), with no significant changes in circularity and area,  
291 acute inhibition of TRPV4 with GSK21 and HC compounds induced a shortening of main branches  
292 and thin ramifications, and prevented cell migration during 24 h treatment with the TRPV4 antagonist  
293 (**Figure 1c-e**, **Figure S1a, b**). Quantitative analysis of morphological parameters revealed that  
294 microglia treated with 10  $\mu$ M GSK21 and HC show significant increased circularity and reduced area  
295 as fast as 30 min after TRPV4 inhibition. In contrast, acute inhibition with RN evoked a short-lasting  
296 decrease of cellular area, with no significant effect in cell circularity.

297 Changes in morphological complexity of microglia treated with a 10 times lower dose of GSK21 were  
298 only evident after 48 h (**Figure 1e**), indicating that TRPV4 inhibition induces branch retraction in a  
299 time- and concentration-dependent manner. Conversely, the effects induced by GSK21 and RN were  
300 significant up to 6 h, with cells recovering their morphological complexity by 24 h incubation time.  
301 In addition, acute inhibition of TRPV4 activity with 10  $\mu$ M GSK21 and HC decreased the percentage  
302 of microglia exhibiting non-directed migration and the total displacement during persistent random  
303 walk (**Figure 1d, f, g**, **Figure S1c**). GSK21 (1  $\mu$ M) was less effective in reducing microglial persistent  
304 random walk, likely a consequence of the late effect on the morphological changes (**Figure 1e, g**).  
305 The transient effect of RN compound did not alter the overall non-directed migration of microglia  
306 (**Figure S1c**).

307 Possible off-target effects from the TRPV4 antagonist were evaluated by comparing morphological  
308 and migratory effects in *Trpv4* KO microglia untreated and treated with GSK21, HC and RN (10  $\mu$ M).  
309 No significant differences were observed on morphology nor percentage of motile cells and total  
310 displacement during persistent random walk (**Figure S2**). Taken together, our results show that  
311 inhibition of TRPV4, but not constitutive absence, reduces microglial process complexity, area and  
312 overall migration *in vitro*.

313

314 **3.2 TRPV4 inhibition reduces microglial tubulin and actin-rich filopodia dynamics *in vitro***  
315 TRPV4 activity regulates cytoskeletal changes in neuronal cells by directly interacting with  
316 microtubules (MT) and actin, thus modifying cell morphology and motility (Goswami *et al.*, 2010).  
317 However, whether similar functional interactions operate in microglia remains to be elucidated. To  
318 evaluate this, we investigated tubulin and actin-rich filopodia dynamics before and after exposure  
319 to the TRPV4 antagonist. First, we used the cell-permeable fluorescent dye SiR-Tubulin to label the  
320 MTs of WT microglia untreated and treated with GSK21 (10  $\mu$ M). Live-cell super-resolution  
321 microscopy revealed highly dynamic MTs in untreated primary microglia (**Supplementary movie**  
322 **1**). Moreover, overlaying consecutive regions of MTs from WT microglia (5 s apart), clearly showed  
323 fast MT displacement over time (**Figure 2a, top left panel**). To further quantify this dynamism, we  
324 used particle image velocimetry (PIV) which allowed for measuring cross correlations in pixel  
325 intensity between regions of two consecutive images in a defined time frame (interrogation area).  
326 PIV analysis provides a range of vector velocities for the selected interrogation areas (**Figure 2b,**  
327 **white bar**) representing the displacement of MTs, as shown in the heatmap of **Figure 2a**. Upon  
328 inhibition of TRPV4, MT dynamism was abrogated (**Figure 2a top right panel, Supplementary**  
329 **movie 2**), with a decreased vector velocity over one frame compared to the untreated cells (**Figure**  
330 **2b**). Quantification of the total time-lapse revealed a reduced cumulative vector velocity in specific  
331 interrogation areas for microglia with acute TRPV4 inhibition, demonstrating the sustained effect of  
332 TRPV4 inhibition over tubulin dynamism (**Figure 2c**). Furthermore, we observed that untreated  
333 microglia exhibit a greater median velocity per frame compared to GSK21-treated microglia (**Figure**  
334 **2d**), indicating a reduction in MT displacement over the entire timespan. Overall, these data show  
335 altered MT dynamics after acutely-inhibiting TRPV4 in primary microglia.  
336 Next, we determined whether the TRPV4 antagonist also affects filopodia dynamics. Since filopodia  
337 are actin-rich structures (Franco-Bocanegra *et al.*, 2019), their dynamical changes are indicative for  
338 the effect of acute TRPV4 inhibition on microglial actin dynamics. We took advantage of the  
339 ubiquitous expression of eGFP in our CX3CR1-eGFP mice to visualize the highly dynamic filopodia  
340 (Gallop, 2020). To assess filopodia number, length and movement, we defined multiple regions of  
341 interest surrounding microglial processes and recorded moving filopodia over a timespan of 2.5 min.  
342 TIC-cultured WT microglia were highly ramified and contained up to fourth order branches that were  
343 enriched with long and highly dynamic filopodia (**Figure 3a, left panel**). Upon treatment with  
344 GSK21 (10  $\mu$ M), the morphological architecture of the main branches remained unaltered (for the  
345 extent of this experiment 2.5 min) (**Figure 3a, right panel**); however, a significant decrease in the  
346 number of filopodia (**Figure 3b**) and their corresponding length (**Figure 3c**) was observed. Filopodia  
347 movement was also reduced after exposure to GSK21 (**Figure 3c & Supplementary movie 3**).  
348 Similarly, acute inhibition with HC and RN compounds decreased the length, number and motility of  
349 thin filopodia structures (**Figure S3**). Altogether, acute inhibition of TRPV4 significantly reduced  
350 filopodia features (**Figure 3b, c**), which subsequently decreased the area scanned by these  
351 structures (**Figure 3e**). In summary, these findings demonstrate that inhibition of TRPV4 reduces  
352 cytoskeletal rearrangements in microglia by decreasing dynamics of both tubulin and actin-rich  
353 filopodia.  
354

### 355 **3.3 *Trpv4* knockout affects microglial morphology and branch motility *in situ***

356 Unlike acute TRPV4 inhibition, *Trpv4* KO primary microglia exhibit migratory and morphological  
357 features *in vitro* that are undistinguishable from WT cells (**Figure 1a, 1b**). It should be noted that  
358 microglia lose part of their gene signature upon isolation from their brain (Bohlen *et al.*, 2017;  
359 Haynes *et al.*, 2006). Hereby, microglial function can slightly differ *in vitro* compared to *in situ*. We  
360 sought to test whether constitutive absence of TRPV4 could affect morphology, density and branch  
361 motility of microglia when present in their natural environment. We thus investigated branch motility  
362 using two-photon live-imaging of CX3CR1-eGFP microglia in acute cortical slices from WT and *Trpv4*  
363 KO mice. We quantified the surveyed area and both process extension and retraction speeds for  
364 total duration of 10 min. These experiments revealed highly dynamic WT microglia continuously  
365 scanning the environment, as represented in the overlaying time consecutive images in **Figure 4a**.  
366 Although *Trpv4* KO microglia displayed dynamic branches, we observed that the branches covered  
367 significantly less area during the same time lapse (2 min) (**Figure 4a, b**). To discern if the impact  
368 on brain area coverage resulted from changes in process motility, we quantified extension and  
369 retraction events by manually tracking motile processes from both WT and *Trpv4* KO microglia. We  
370 observed that retraction speed was not affected between both genotypes; however, lack of TRPV4  
371 did significantly decrease process extension speed (**Figure 4c**).

372 Next, we probed for possible contributions in microglial density and morphological complexity after  
373 constitutive loss of TRPV4. We perfusion-fixed P21 WT and *Trpv4* KO mice and quantified microglial  
374 density in layers 1, 2/3 and 5 of the primary and secondary motor areas. Both WT and *Trpv4* KO  
375 mice exhibited a homogenous distribution of microglia throughout the brain, with no differences  
376 observed between both genotypes (**Figure 5a, b**). Finally, we analyzed microglia process  
377 ramification in the cortex by performing a three-dimensional Sholl analysis, from which the  
378 outcoming cell skeletons of *Trpv4* KO microglia showed an aberrant reduction in morphological  
379 complexity (**Figure 5c**). High-resolution confocal microscopy confirmed these changes and revealed  
380 a reduced ramification and number of tips in microglia lacking TRPV4 (**Figure 5d**). Furthermore,  
381 Sholl quantification displayed fewer branching points and shorter processes in *Trpv4* KO microglia  
382 compared to their WT littermates (**Figure 5e**). Thus, in contrast to density, *in situ* microglia lacking  
383 TRPV4 exhibit a reduced process extension speed, likely contributing to both a decreased process  
384 complexity and brain surveillance.

385

#### 386 **4. DISCUSSION (Word count: 960)**

387 In microglia, Ca<sup>2+</sup>-driven cell movement has been proven to be pivotal for proper brain development  
388 and maintaining homeostasis (Sharma & Ping, 2014); however, the mechanisms behind this process  
389 remain unknown. Recently, microglial TRPV4 was shown to be involved in the signaling and  
390 morphological changes in response to hypoosmotic conditions and pharmacological modulators  
391 (Chakraborty & Goswami, 2022; Redmon *et al.*, 2021) and temperature-dependent movement of  
392 microglia both *in vitro* and *in vivo* (Nishimoto *et al.*, 2021). Despite this increasing role for TRPV4 in  
393 microglia, its role on cytoskeleton remodeling necessary for microglial architecture and motility  
394 remains to be elucidated. Using live-cell imaging techniques *in vitro* and *in situ*, we here confirmed  
395 that TRPV4 activity regulates microglial morphology and migration. More importantly, we  
396 demonstrate that acute inhibition of TRPV4 directly affect remodeling of actin and tubulin  
397 cytoskeleton in microglia.

398 Using three different antagonists we demonstrate that acute TRPV4 inhibition evokes immediate  
399 changes in microglial morphology and branch motility. However, inhibition-induced long-lasting  
400 effects were variable among the compounds, most likely dependent on individual inhibition potency,  
401 solubility and stability properties.

402 To get insight into the possible mechanisms underpinning microglial motion, we analyzed tubulin and  
403 actin-rich filopodia dynamics before and after acute inhibition of TRPV4. Pharmacological inhibition  
404 of TRPV4 caused a significant decrease in both tubulin- and actin-dependent motion showing less  
405 dynamic MTs and decreased filopodia number and length. Consistent with these data, we found that  
406 acute inhibition of TRPV4 significantly reduced the area scanned by filopodia, a result correlated with  
407 the decreased filopodia features.

408 Our findings raise the question on how the channel can steer cytoskeleton remodeling in microglial  
409 cells. In light of previous studies, we speculate that the TRPV4-mediated Ca<sup>2+</sup> influx contributes to  
410 the upregulation and recruitment of proteins necessary for cytoskeleton remodeling (Sharma & Ping,  
411 2014; Tsai *et al.*, 2015; Tsai & Meyer, 2012; Wei *et al.*, 2009). Similar mechanisms are found in  
412 endometrial cancer cells, for instance, where TRPV4 regulates cytoskeleton rearrangements by  
413 mediating Ca<sup>2+</sup>-influxes that activate the RhoA/ROCK1 pathway which in turn upregulates F-actin  
414 and paxillin, an actin-binding protein (Li *et al.*, 2020). On the other hand, TRPV4 activity promotes  
415 the activation of Rac1, a small GTPase involved in cell migration, by targeting AKT phosphorylation  
416 and thereby enhancing glioma cell motility (Ou-Yang *et al.*, 2018). Importantly, TRPV4 interacts  
417 directly with actin, tubulin and neurofilament proteins through its C-terminus, and the receptor  
418 colocalizes with actin-rich structures such as filopodia, lamellipodia and focal adhesion points,  
419 thereby regulating cell morphology and net movement of neurites (Goswami *et al.*, 2010). Taken  
420 together, we present pharmacological evidence demonstrating that TRPV4 inhibition is correlated  
421 with reduced cytoskeleton remodeling.

422 In our experiments, the constitutive absence of functional TRPV4 failed to alter microglia morphology  
423 and displacement *in vitro*. Although this is contradiction with previous results showing reduced  
424 microglial migration in *Trpv4* KO microglia (Nishimoto *et al.*, 2021), there are important differences  
425 regarding mouse age, isolation protocol and culture conditions to consider. Unlike previous *in vitro*  
426 results using *Trpv4* KO microglia, we isolate microglia from postnatal day 21 mice, an age when  
427 murine microglia have acquired their mature transcriptomic signature (Bennett *et al.*, 2016;

428 Matcovitch-Natan *et al.*, 2016). For these cultures, substrate coating is essential for cell survival and  
429 the development of morphological features and dynamics that mimics resting microglia (Bohlen *et*  
430 *al.*, 2017). In this condition, cultured microglia are sensitive to topological and mechanical properties  
431 of the substrate (Bollmann *et al.*, 2015), likely involving redundant intracellular signaling from  
432 mechanosensitive channels. This includes several other Ca<sup>2+</sup>-permeable channels involved in cell  
433 migration. For instance, TRPM7 and TRPM2 are correlated with Ca<sup>2+</sup>-driven cell movement (Almasi  
434 *et al.*, 2019; Jiang *et al.*, 2003; Nishimoto *et al.*, 2021; Wei *et al.*, 2009), and mechanically-gated  
435 Piezo channels with a pivotal role in cell migration by regulating actin structures and modifying cell  
436 shape through cation influx (Canales Coutino & Mayor, 2021; Mousawi *et al.*, 2020). We found that  
437 TRPM2, TRPM7 and Piezo channels are not differentially-regulated in *Trpv4* KO microglia (**Figure**  
438 **S4**). Our results indicate that the basal expression of these channels is sufficient to compensate for  
439 the constitutive lack of TRPV4, but not for the immediate, acute inhibition of TRPV4. Altogether,  
440 these findings suggest that, although the functional TRPV4 activity might be redundant, it  
441 outbalances other Ca<sup>2+</sup>-permeable channels in the homeostatic regulation of cytoskeletal dynamism.  
442 Microglia within the brain parenchyma interact with a vast diversity of extracellular matrix  
443 components present in the perineural nets (e.g. proteoglycan, tenascin R) and the neural interstitial  
444 matrix (e.g. collagen, fibronectin, laminin) predominantly through GPCR and integrin receptors, both  
445 acting as endogenous modulators of TRPV4 activity (Matthews *et al.*, 2010; Saifeddine *et al.*, 2015).  
446 This might increase the specific dependence of TRPV4 signaling, resulting in the reduced  
447 ramifications, shorter branches and less branching points observed *in situ*.  
448 It should be noted that microglia can sense and respond to changes in neuronal activity (Umpierre  
449 *et al.*, 2020; Umpierre & Wu, 2021) and that neuronal cells express TRPV4 on their plasma  
450 membrane (Goswami *et al.*, 2010; Kanju & Liedtke, 2016). Therefore, the absence of TRPV4 in  
451 microglial cells may be influenced by the overall lack of TRPV4 in other brain cells. Yet, our *in vitro*  
452 experiments prove a cell-autonomous role for TRPV4 in microglia. Alternative approaches such as  
453 the Cre-Lox system or a bone marrow chimera (Cronk *et al.*, 2018) with microglia-specific *Trpv4*  
454 deficiency could provide supportive information regarding microglia cell-specific effects.  
455 In conclusion, our results demonstrate that the mechanosensitive Ca<sup>2+</sup>-permeable channel TRPV4  
456 contributes to the regulation of the actin and MT cytoskeleton in microglia consequently steering  
457 morphological complexity and movement of the cells. The significance of this research is substantial  
458 as it provides novel insights into the link between cytoskeletal dynamism and ion channels in  
459 microglial properties and hereby contributes to unravelling cellular and molecular mechanisms  
460 underpinning proper microglial function.  
461

462 **5. REFERENCES**

- 463 Almasi, S., Sterea, A. M., Fernando, W., Clements, D. R., Marcato, P., Hoskin, D. W., Gujar, S., & El  
464 Hiani, Y. (2019). TRPM2 ion channel promotes gastric cancer migration, invasion and tumor growth  
465 through the AKT signaling pathway. *Sci Rep*, *9*(1), 4182. doi:10.1038/s41598-019-40330-1
- 466 Becker, D., Blase, C., Bereiter-Hahn, J., & Jendrach, M. (2005). TRPV4 exhibits a functional role in  
467 cell-volume regulation. *J Cell Sci*, *118*(Pt 11), 2435-2440. doi:10.1242/jcs.02372
- 468 Bennett, M. L., Bennett, F. C., Liddelow, S. A., Ajami, B., Zamanian, J. L., Fernhoff, N. B., Mulinyawe,  
469 S. B., Bohlen, C. J., Adil, A., Tucker, A., Weissman, I. L., Chang, E. F., Li, G., Grant, G. A., Hayden  
470 Gephart, M. G., & Barres, B. A. (2016). New tools for studying microglia in the mouse and human  
471 CNS. *Proc Natl Acad Sci U S A*, *113*(12), E1738-1746. doi:10.1073/pnas.1525528113
- 472 Bernier, L. P., Bohlen, C. J., York, E. M., Choi, H. B., Kamyabi, A., Dissing-Olesen, L., Hefendehl, J.  
473 K., Collins, H. Y., Stevens, B., Barres, B. A., & MacVicar, B. A. (2019). Nanoscale Surveillance of  
474 the Brain by Microglia via cAMP-Regulated Filopodia. *Cell Rep*, *27*(10), 2895-2908 e2894.  
475 doi:10.1016/j.celrep.2019.05.010
- 476 Bohlen, C. J., Bennett, F. C., Tucker, A. F., Collins, H. Y., Mulinyawe, S. B., & Barres, B. A. (2017).  
477 Diverse Requirements for Microglial Survival, Specification, and Function Revealed by Defined-  
478 Medium Cultures. *Neuron*, *94*(4), 759-773 e758. doi:10.1016/j.neuron.2017.04.043
- 479 Bollmann, L., Koser, D. E., Shahapure, R., Gautier, H. O., Holzapfel, G. A., Scarcelli, G., Gather, M.  
480 C., Ulbricht, E., & Franze, K. (2015). Microglia mechanics: immune activation alters traction forces  
481 and durotaxis. *Front Cell Neurosci*, *9*, 363. doi:10.3389/fncel.2015.00363
- 482 Canales Coutino, B., & Mayor, R. (2021). Mechanosensitive ion channels in cell migration. *Cells Dev*,  
483 *166*, 203683. doi:10.1016/j.cdev.2021.203683
- 484 Canales, J., Morales, D., Blanco, C., Rivas, J., Diaz, N., Angelopoulos, I., & Cerda, O. (2019). A  
485 TR(i)P to Cell Migration: New Roles of TRP Channels in Mechanotransduction and Cancer. *Front*  
486 *Physiol*, *10*, 757. doi:10.3389/fphys.2019.00757
- 487 Chakraborty, R., & Goswami, C. (2022). Both heat-sensitive TRPV4 and cold-sensitive TRPM8 ion  
488 channels regulate microglial activity. *Biochem Biophys Res Commun*, *611*, 132-139.  
489 doi:10.1016/j.bbrc.2022.04.032
- 490 Clapham, D. E. (2003). TRP channels as cellular sensors. *Nature*, *426*(6966), 517-524.  
491 doi:10.1038/nature02196
- 492 Colonna, M., & Butovsky, O. (2017). Microglia Function in the Central Nervous System During Health  
493 and Neurodegeneration. *Annu Rev Immunol*, *35*, 441-468. doi:10.1146/annurev-immunol-  
494 051116-052358
- 495 Cronk, J. C., Filiano, A. J., Louveau, A., Marin, I., Marsh, R., Ji, E., Goldman, D. H., Smirnov, I.,  
496 Geraci, N., Acton, S., Overall, C. C., & Kipnis, J. (2018). Peripherally derived macrophages can  
497 engraft the brain independent of irradiation and maintain an identity distinct from microglia. *J Exp*  
498 *Med*, *215*(6), 1627-1647. doi:10.1084/jem.20180247
- 499 Dutta, B., Arya, R. K., Goswami, R., Alharbi, M. O., Sharma, S., & Rahaman, S. O. (2020). Role of  
500 macrophage TRPV4 in inflammation. *Lab Invest*, *100*(2), 178-185. doi:10.1038/s41374-019-0334-  
501 6
- 502 Echeverry, S., Rodriguez, M. J., & Torres, Y. P. (2016). Transient Receptor Potential Channels in  
503 Microglia: Roles in Physiology and Disease. *Neurotox Res*, *30*(3), 467-478. doi:10.1007/s12640-  
504 016-9632-6
- 505 Eyo, U. B., Peng, J., Swiatkowski, P., Mukherjee, A., Bispo, A., & Wu, L. J. (2014). Neuronal  
506 hyperactivity recruits microglial processes via neuronal NMDA receptors and microglial P2Y12  
507 receptors after status epilepticus. *J Neurosci*, *34*(32), 10528-10540.  
508 doi:10.1523/JNEUROSCI.0416-14.2014
- 509 Franco-Bocanegra, D. K., McAuley, C., Nicoll, J. A. R., & Boche, D. (2019). Molecular Mechanisms of  
510 Microglial Motility: Changes in Ageing and Alzheimer's Disease. *Cells*, *8*(6).  
511 doi:10.3390/cells8060639
- 512 Gallop, J. L. (2020). Filopodia and their links with membrane traffic and cell adhesion. *Semin Cell*  
513 *Dev Biol*, *102*, 81-89. doi:10.1016/j.semcdb.2019.11.017

- 514 Goswami, C., Kuhn, J., Heppenstall, P. A., & Hucho, T. (2010). Importance of non-selective cation  
515 channel TRPV4 interaction with cytoskeleton and their reciprocal regulations in cultured cells. *PLoS*  
516 *One*, 5(7), e11654. doi:10.1371/journal.pone.0011654
- 517 Haynes, S. E., Hollopeter, G., Yang, G., Kurpius, D., Dailey, M. E., Gan, W. B., & Julius, D. (2006).  
518 The P2Y12 receptor regulates microglial activation by extracellular nucleotides. *Nat Neurosci*,  
519 9(12), 1512-1519. doi:10.1038/nn1805
- 520 Hines, D. J., Hines, R. M., Mulligan, S. J., & Macvicar, B. A. (2009). Microglia processes block the  
521 spread of damage in the brain and require functional chloride channels. *Glia*, 57(15), 1610-1618.  
522 doi:10.1002/glia.20874
- 523 Jiang, X., Newell, E. W., & Schlichter, L. C. (2003). Regulation of a TRPM7-like current in rat brain  
524 microglia. *J Biol Chem*, 278(44), 42867-42876. doi:10.1074/jbc.M304487200
- 525 Jung, S., Aliberti, J., Graemmel, P., Sunshine, M. J., Kreutzberg, G. W., Sher, A., & Littman, D. R.  
526 (2000). Analysis of fractalkine receptor CX(3)CR1 function by targeted deletion and green  
527 fluorescent protein reporter gene insertion. *Mol Cell Biol*, 20(11), 4106-4114.  
528 doi:10.1128/MCB.20.11.4106-4114.2000
- 529 Kanju, P., & Liedtke, W. (2016). Pleiotropic function of TRPV4 ion channels in the central nervous  
530 system. *Exp Physiol*, 101(12), 1472-1476. doi:10.1113/EP085790
- 531 Konno, M., Shirakawa, H., Iida, S., Sakimoto, S., Matsutani, I., Miyake, T., Kageyama, K.,  
532 Nakagawa, T., Shibasaki, K., & Kaneko, S. (2012). Stimulation of transient receptor potential  
533 vanilloid 4 channel suppresses abnormal activation of microglia induced by lipopolysaccharide. *Glia*,  
534 60(5), 761-770. doi:10.1002/glia.22306
- 535 Kyrargyri, V., Madry, C., Rifat, A., Arancibia-Carcamo, I. L., Jones, S. P., Chan, V. T. T., Xu, Y.,  
536 Robaye, B., & Attwell, D. (2020). P2Y13 receptors regulate microglial morphology, surveillance,  
537 and resting levels of interleukin 1beta release. *Glia*, 68(2), 328-344. doi:10.1002/glia.23719
- 538 Li, X., Cheng, Y., Wang, Z., Zhou, J., Jia, Y., He, X., Zhao, L., Dong, Y., Fan, Y., Yang, X., Shen, B.,  
539 Wu, X., Wang, J., Xiong, C., Wei, L., Li, X., & Wang, J. (2020). Calcium and TRPV4 promote  
540 metastasis by regulating cytoskeleton through the RhoA/ROCK1 pathway in endometrial cancer.  
541 *Cell Death Dis*, 11(11), 1009. doi:10.1038/s41419-020-03181-7
- 542 Liu, C., & Montell, C. (2015). Forcing open TRP channels: Mechanical gating as a unifying activation  
543 mechanism. *Biochem Biophys Res Commun*, 460(1), 22-25. doi:10.1016/j.bbrc.2015.02.067
- 544 Madry, C., & Attwell, D. (2015). Receptors, ion channels, and signaling mechanisms underlying  
545 microglial dynamics. *J Biol Chem*, 290(20), 12443-12450. doi:10.1074/jbc.R115.637157
- 546 Matcovitch-Natan, O., Winter, D. R., Giladi, A., Vargas Aguilar, S., Spinrad, A., Sarrazin, S., Ben-  
547 Yehuda, H., David, E., Zelada Gonzalez, F., Perrin, P., Keren-Shaul, H., Gury, M., Lara-Astaiso, D.,  
548 Thaiss, C. A., Cohen, M., Bahar Halpern, K., Baruch, K., Deczkowska, A., Lorenzo-Vivas, E.,  
549 Itzkovitz, S., Elinav, E., Sieweke, M. H., Schwartz, M., & Amit, I. (2016). Microglia development  
550 follows a stepwise program to regulate brain homeostasis. *Science*, 353(6301), aad8670.  
551 doi:10.1126/science.aad8670
- 552 Matthews, B. D., Thodeti, C. K., Tytell, J. D., Mammoto, A., Overby, D. R., & Ingber, D. E. (2010).  
553 Ultra-rapid activation of TRPV4 ion channels by mechanical forces applied to cell surface beta1  
554 integrins. *Integr Biol (Camb)*, 2(9), 435-442. doi:10.1039/c0ib00034e
- 555 Meijering, E., Dzyubachyk, O., & Smal, I. (2012). Methods for cell and particle tracking. *Methods*  
556 *Enzymol*, 504, 183-200. doi:10.1016/B978-0-12-391857-4.00009-4
- 557 Michalick, L., & Kuebler, W. M. (2020). TRPV4-A Missing Link Between Mechanosensation and  
558 Immunity. *Front Immunol*, 11, 413. doi:10.3389/fimmu.2020.00413
- 559 Mizoguchi, Y., Kato, T. A., Seki, Y., Ohgidani, M., Sagata, N., Horikawa, H., Yamauchi, Y., Sato-  
560 Kasai, M., Hayakawa, K., Inoue, R., Kanba, S., & Monji, A. (2014). Brain-derived neurotrophic  
561 factor (BDNF) induces sustained intracellular Ca<sup>2+</sup> elevation through the up-regulation of surface  
562 transient receptor potential 3 (TRPC3) channels in rodent microglia. *J Biol Chem*, 289(26), 18549-  
563 18555. doi:10.1074/jbc.M114.555334
- 564 Mousawi, F., Peng, H., Li, J., Ponnambalam, S., Roger, S., Zhao, H., Yang, X., & Jiang, L. H. (2020).  
565 Chemical activation of the Piezo1 channel drives mesenchymal stem cell migration via inducing



566 ATP release and activation of P2 receptor purinergic signaling. *Stem Cells*, 38(3), 410-421.  
567 doi:10.1002/stem.3114

568 Nilius, B., & Owsianik, G. (2011). The transient receptor potential family of ion channels. *Genome*  
569 *Biol*, 12(3), 218. doi:10.1186/gb-2011-12-3-218

570 Nimmerjahn, A., Kirchhoff, F., & Helmchen, F. (2005). Resting microglial cells are highly dynamic  
571 surveillants of brain parenchyma in vivo. *Science*, 308(5726), 1314-1318.  
572 doi:10.1126/science.1110647

573 Nishimoto, R., Derouiche, S., Eto, K., Devenci, A., Kashio, M., Kimori, Y., Matsuoka, Y., Morimatsu,  
574 H., Nabekura, J., & Tominaga, M. (2021). Thermosensitive TRPV4 channels mediate temperature-  
575 dependent microglia movement. *Proc Natl Acad Sci U S A*, 118(17). doi:10.1073/pnas.2012894118

576 Ohsawa, K., & Kohsaka, S. (2011). Dynamic motility of microglia: purinergic modulation of microglial  
577 movement in the normal and pathological brain. *Glia*, 59(12), 1793-1799. doi:10.1002/glia.21238

578 Ou-Yang, Q., Li, B., Xu, M., & Liang, H. (2018). TRPV4 promotes the migration and invasion of  
579 glioma cells via AKT/Rac1 signaling. *Biochem Biophys Res Commun*, 503(2), 876-881.  
580 doi:10.1016/j.bbrc.2018.06.090

581 Redmon, S. N., Yarishkin, O., Lakk, M., Jo, A., Mustafic, E., Tvrdik, P., & Krizaj, D. (2021). TRPV4  
582 channels mediate the mechanoreponse in retinal microglia. *Glia*, 69(6), 1563-1582.  
583 doi:10.1002/glia.23979

584 Ryskamp, D. A., Frye, A. M., Phuong, T. T., Yarishkin, O., Jo, A. O., Xu, Y., Lakk, M., Iuso, A.,  
585 Redmon, S. N., Ambati, B., Hageman, G., Prestwich, G. D., Torrejon, K. Y., & Krizaj, D. (2016).  
586 TRPV4 regulates calcium homeostasis, cytoskeletal remodeling, conventional outflow and  
587 intraocular pressure in the mammalian eye. *Sci Rep*, 6, 30583. doi:10.1038/srep30583

588 Saifeddine, M., El-Daly, M., Mihara, K., Bunnnett, N. W., McIntyre, P., Altier, C., Hollenberg, M. D., &  
589 Ramachandran, R. (2015). GPCR-mediated EGF receptor transactivation regulates TRPV4 action in  
590 the vasculature. *Br J Pharmacol*, 172(10), 2493-2506. doi:10.1111/bph.13072

591 Salter, M. W., & Stevens, B. (2017). Microglia emerge as central players in brain disease. *Nat Med*,  
592 23(9), 1018-1027. doi:10.1038/nm.4397

593 Sappington, R. M., & Calkins, D. J. (2008). Contribution of TRPV1 to microglia-derived IL-6 and  
594 NFkappaB translocation with elevated hydrostatic pressure. *Invest Ophthalmol Vis Sci*, 49(7),  
595 3004-3017. doi:10.1167/iovs.07-1355

596 Schiefer, J., Kampe, K., Dodt, H. U., Zieglgansberger, W., & Kreutzberg, G. W. (1999). Microglial  
597 motility in the rat facial nucleus following peripheral axotomy. *J Neurocytol*, 28(6), 439-453.  
598 doi:10.1023/a:1007048903862

599 Schindelin, J., Arganda-Carreras, I., Frise, E., Kaynig, V., Longair, M., Pietzsch, T., Preibisch, S.,  
600 Rueden, C., Saalfeld, S., Schmid, B., Tinevez, J. Y., White, D. J., Hartenstein, V., Eliceiri, K.,  
601 Tomancak, P., & Cardona, A. (2012). Fiji: an open-source platform for biological-image analysis.  
602 *Nat Methods*, 9(7), 676-682. doi:10.1038/nmeth.2019

603 Sharma, P., & Ping, L. (2014). Calcium ion influx in microglial cells: physiological and therapeutic  
604 significance. *J Neurosci Res*, 92(4), 409-423. doi:10.1002/jnr.23344

605 Smolders, S. M., Kessels, S., Vanganswinkel, T., Rigo, J. M., Legendre, P., & Brone, B. (2019).  
606 Microglia: Brain cells on the move. *Prog Neurobiol*, 178, 101612.  
607 doi:10.1016/j.pneurobio.2019.04.001

608 Stark, J. C., Wallace, E., Lim, R., & Leaw, B. (2018). Characterization and Isolation of Mouse Primary  
609 Microglia by Density Gradient Centrifugation. *J Vis Exp*(132). doi:10.3791/57065

610 Sun, Y., Chauhan, A., Sukumaran, P., Sharma, J., Singh, B. B., & Mishra, B. B. (2014). Inhibition of  
611 store-operated calcium entry in microglia by helminth factors: implications for immune suppression  
612 in neurocysticercosis. *J Neuroinflammation*, 11, 210. doi:10.1186/s12974-014-0210-7

613 Swiatkowski, P., Murugan, M., Eyo, U. B., Wang, Y., Rangaraju, S., Oh, S. B., & Wu, L. J. (2016).  
614 Activation of microglial P2Y12 receptor is required for outward potassium currents in response to  
615 neuronal injury. *Neuroscience*, 318, 22-33. doi:10.1016/j.neuroscience.2016.01.008

616 Thevenaz, P., Ruttimann, U. E., & Unser, M. (1998). A pyramid approach to subpixel registration  
617 based on intensity. *IEEE Trans Image Process*, 7(1), 27-41. doi:10.1109/83.650848

618 Thielicke, W., & Stamhuis, E. J. (2014). PIVlab – Towards User-friendly, Affordable and Accurate  
619 Digital Particle Image Velocimetry in MATLAB. *J. Open Res. Softw.*, 2(1), p.e30. doi:  
620 <http://doi.org/10.5334/jors.bl>

621 Tsai, F. C., Kuo, G. H., Chang, S. W., & Tsai, P. J. (2015). Ca<sup>2+</sup> signaling in cytoskeletal  
622 reorganization, cell migration, and cancer metastasis. *Biomed Res Int*, 2015, 409245.  
623 doi:10.1155/2015/409245

624 Tsai, F. C., & Meyer, T. (2012). Ca<sup>2+</sup> pulses control local cycles of lamellipodia retraction and  
625 adhesion along the front of migrating cells. *Curr Biol*, 22(9), 837-842.  
626 doi:10.1016/j.cub.2012.03.037

627 Umpierre, A. D., Bystrom, L. L., Ying, Y., Liu, Y. U., Worrell, G., & Wu, L. J. (2020). Microglial calcium  
628 signaling is attuned to neuronal activity in awake mice. *Elife*, 9. doi:10.7554/eLife.56502

629 Umpierre, A. D., & Wu, L. J. (2021). How microglia sense and regulate neuronal activity. *Glia*, 69(7),  
630 1637-1653. doi:10.1002/glia.23961

631 Wei, C., Wang, X., Chen, M., Ouyang, K., Song, L. S., & Cheng, H. (2009). Calcium flickers steer  
632 cell migration. *Nature*, 457(7231), 901-905. doi:10.1038/nature07577

633 Wolf, S. A., Boddeke, H. W., & Kettenmann, H. (2017). Microglia in Physiology and Disease. *Annu*  
634 *Rev Physiol*, 79, 619-643. doi:10.1146/annurev-physiol-022516-034406

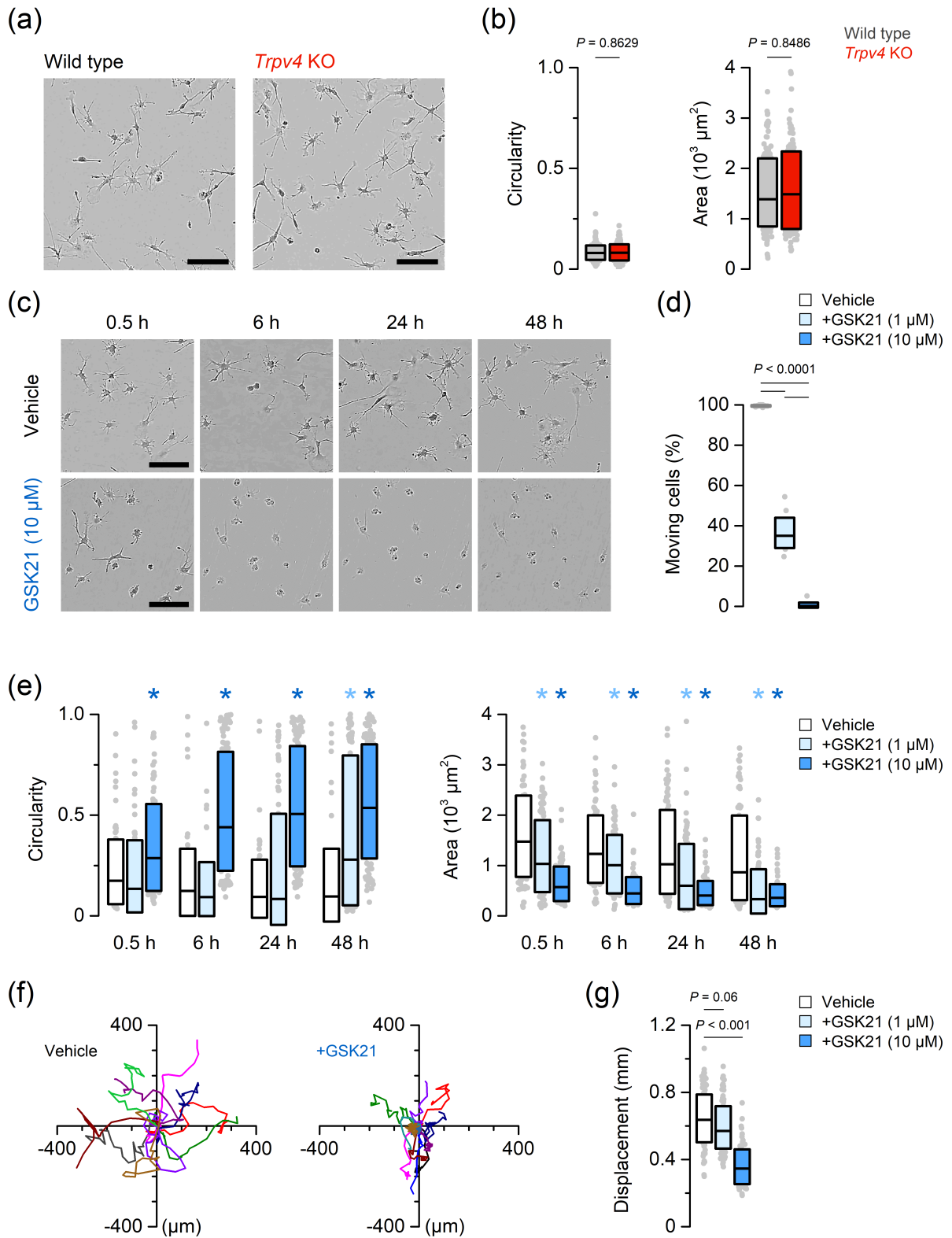
635 Xiao, H., & Peng, H. (2013). APP2: automatic tracing of 3D neuron morphology based on hierarchical  
636 pruning of a gray-weighted image distance-tree. *Bioinformatics*, 29(11), 1448-1454.  
637 doi:10.1093/bioinformatics/btt170

638

639

640

641

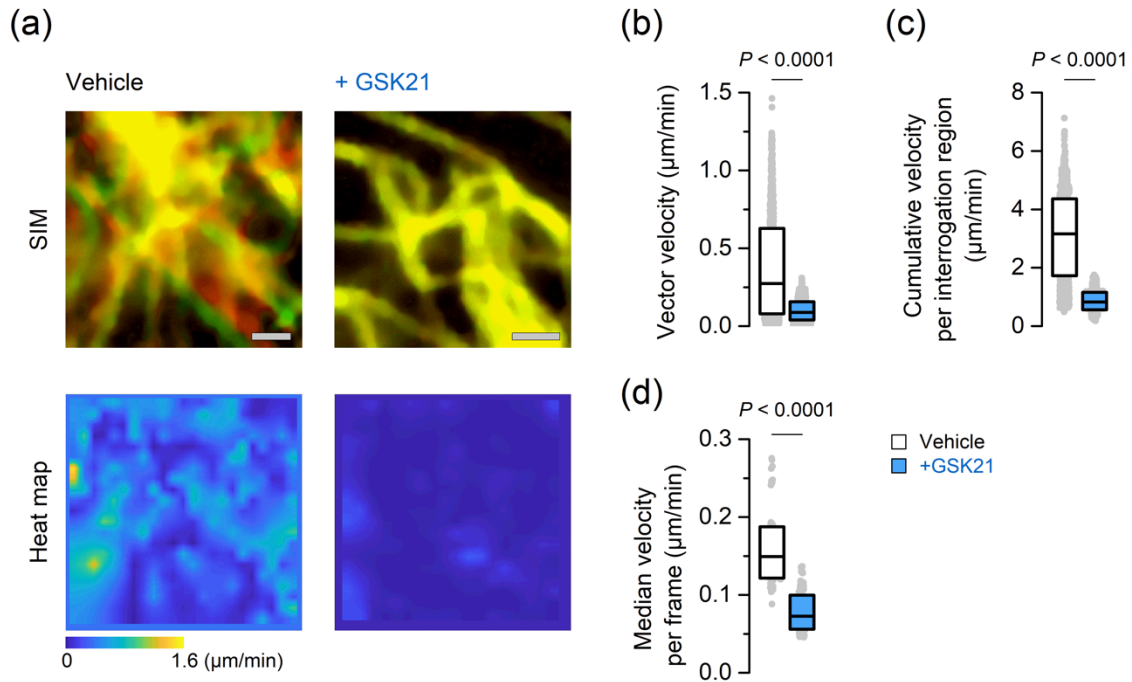


643

644 **FIGURE 1** Acute inhibition of TRPV4 triggers morphological and migratory changes on primary microglia *in vitro*.

645 (a) Representative brightfield images of WT and *Trpv4* KO primary microglia after 7 days in culture in collagen-

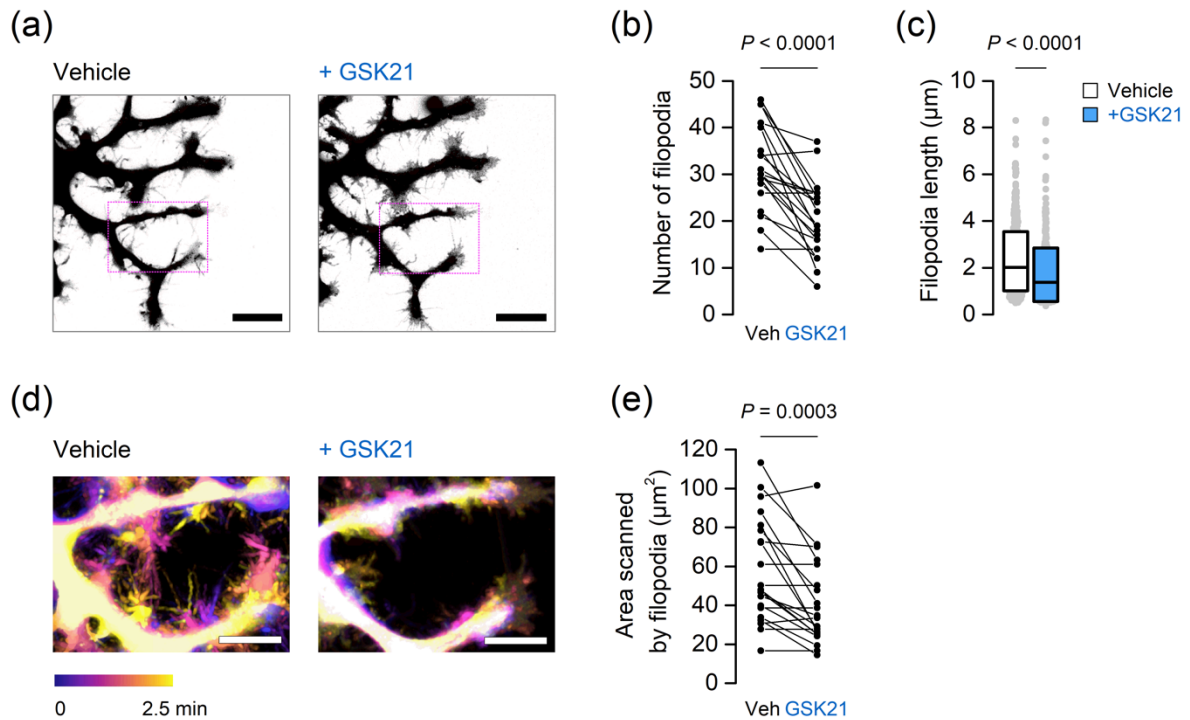
646 coated plates with TIC medium. Scale bar, 100  $\mu\text{m}$ . (b) Circularity and area from WT and *Trpv4* KO microglia  
647 were analyzed using Fiji software. Quantification revealed no morphological differences between both genotypes  
648 ( $n \geq 150$  per genotype, two-tailed Mann-Whitney *U* test). (c) Representative brightfield images of WT primary  
649 microglia at different time points after addition of vehicle (0.2% DMSO) or GSK21 (10  $\mu\text{M}$ ). Scale bar, 100  $\mu\text{m}$ .  
650 (d) Percentage of actively moving microglia 24 h after incubation with vehicle or GSK21 (1  $\mu\text{M}$  and 10  $\mu\text{M}$ ). Data  
651 points (16 per condition,  $n \geq 1300$  cells) represent one quantified field of view (FOV, 1745 x 1289  $\mu\text{m}$ ). FOVs  
652 were randomly selected from different wells from at least 2 independent experiments.  $P < 0.0001$  for all paired  
653 comparisons, two-tailed Fisher's exact test. (e) Circularity and area parameters on primary microglia after acute  
654 inhibition of TRPV4 (GSK21, 1  $\mu\text{M}$  and 10  $\mu\text{M}$ ). Asterisks indicate statistically significant differences (of at least  $P$   
655  $< 0.05$ ) to the untreated cells (Vehicle). Two-tailed Dunn's multiple comparison test,  $n \geq 100$  per condition.  
656 Exact  $P$  values for all paired comparison are listed in **Table S1**. (f) Representative persistent random walk traces  
657 of WT microglia untreated and treated with the TRPV4 inhibitor (GSK21, 10  $\mu\text{M}$ ). (g) Total displacement in 24 h  
658 during persistent random walk of untreated and GSK21-treated (1  $\mu\text{M}$  and 10  $\mu\text{M}$ ) primary microglia. Two-tailed  
659 Dunn's multiple comparison test,  $n \geq 92$  cells per condition.  
660



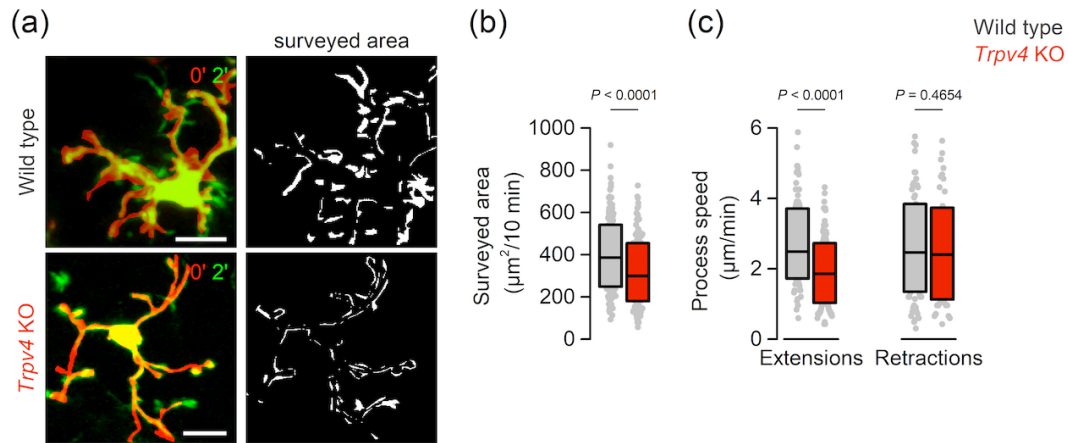
661

662 **FIGURE 2** Dynamism of microglial tubulin decreases upon pharmacological inhibition of TRPV4. (a)  
 663 Representative structure illumination microscopy (SIM) images of tubulin structures (upper panel) recorded in  
 664 WT and TRPV4-inhibited (GSK21) microglia. Green and red colours represent two consecutive images taken 5  
 665 sec apart. Scale bar, 1 µm. PIVlab-generated heat maps of particle vector velocity calculation are shown below  
 666 the corresponding SIM image. The colour-coded bar indicates the range of vector velocity magnitude. (b)  
 667 Vector velocity values of all interrogation areas of the representative images for control and GSK21-treated microglia  
 668 shown in (a). (c) Cumulative velocity values per interrogation area of the representative experiment during 1  
 669 min of recording. (d) Median vector velocity value per time frame. Data points represent individually analyzed  
 670 images ( $n \geq 153$  regions per condition, from two independent experiments). (b-d) Two-tailed Mann Whitney  $U$   
 671 test.

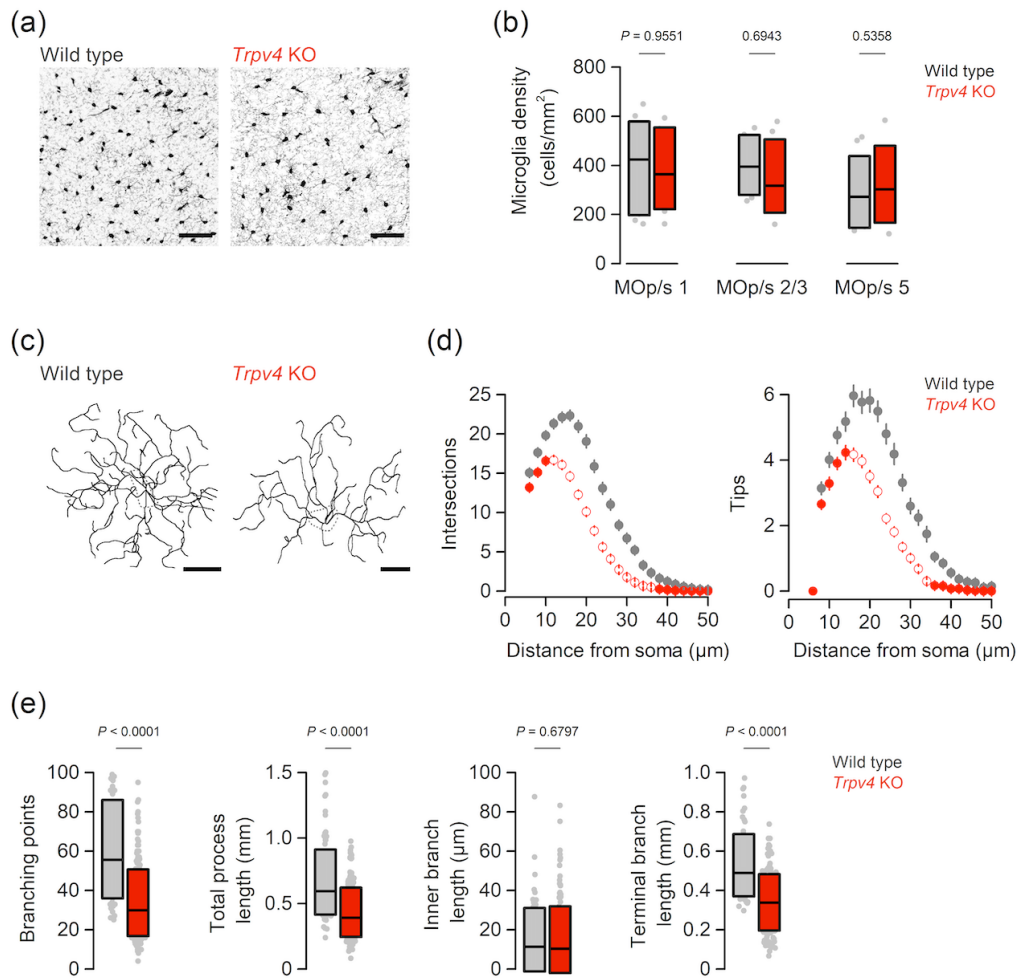
672



673  
 674 **FIGURE 3** Acute inhibition of TRPV4 affects length and motility of actin-rich filopodia in microglia. (a)  
 675 Representative Airyscan images of selected regions in untreated and GSK21-treated microglia. The selection in  
 676 magenta corresponds to the image shown in (d). Scale bar, 10 µm. (b) Number of filopodia during incubation  
 677 with vehicle (0.2% DMSO) and after acute inhibition of TRPV4 (GSK21). Data points represent individual regions  
 678 (n = 21) from 5 cells. Wilcoxon matched-pairs signed rank test. (c) Length of filopodia before (0.2% DMSO,  
 679 Vehicle) and after acute inhibition of TRPV4 (GSK21). Data points represent individual filopodia (n ≥ 430). Two-  
 680 tailed Mann Whitney U test. (d) Temporal colour-coded overlaid images of the area represented in (a) (magenta  
 681 rectangle) for microglia before and after acute inhibition of TRPV4. The colour-coded bar indicates the time range.  
 682 Scale bar embedded, 5 µm. (e) Total scanned area by filopodia in selected regions (n = 21; 5 cells). Wilcoxon  
 683 matched-pairs signed rank test.  
 684



685  
 686 **FIGURE 4** Constitutive absence of TRPV4 affects microglial brain surveillance *in situ*. (a) Representative two-  
 687 photon microscopy images of CX3CR1<sup>eGFP/+</sup> WT and *Trpv4* KO cortical microglia in acute brain slices. Images taken  
 688 2 min apart are overlaid with two different colours (red: 0 min, green: 2 min). Scale bar, 10 μm. The panels on  
 689 the right represent the difference between the two images (2'(green) - 0'(red)). (b) Total surveyed area by  
 690 CX3CR1<sup>eGFP/+</sup> WT (n = 211 cells) and *Trpv4* KO (n = 179 cells) cortical microglia in acute brain slices. (c) Speed  
 691 of process extension and retraction events in CX3CR1<sup>eGFP/+</sup> WT and *Trpv4* KO cortical microglia. The speed of  
 692 extension (n ≥ 139 per genotype) and retraction (n ≥ 69 per genotype) events were quantified from at least 5  
 693 independent slices/mice. (b, c) Two-tailed Mann Whitney U test.  
 694



695

696

697

698

699

700

701

702

703

704

705

706

707

**FIGURE 5** *Trpv4* KO microglia exhibit decreased branch ramifications *in situ*. (a) Representative confocal images of perfusion-fixed P21 CX3CR1<sup>eGFP/+</sup> WT and *Trpv4* KO cortical brain slices. Scale bar, 50 μm. (b) Average microglial density in layer 1, 2/3 and 5 of the primary and secondary motor areas (MOp/s) of the cortex from CX3CR1<sup>eGFP/+</sup> WT (n = 8) and *Trpv4* KO (n = 7) brains. (c) Representative 3D skeletonized microglia obtained from P21 CX3CR1<sup>eGFP/+</sup> WT and *Trpv4* KO mice. The dotted line represents the somatic area. Scale bar, 10 μm. (d, e) Ramification analysis of microglia from perfusion-fixed WT (112 cells, 5 animals) and *Trpv4* KO (193 cells, 5 animals) mice showing Sholl analysis-derived average number of process intersections and tips (d), and number of branching points, total process length, inner branch length and terminal branch length (e) per individual microglia. Empty data points in (d) indicate significant differences ( $P < 0.0001$ , multiple Mann-Whitney *U* test) from equidistant value in WT. Data in (d) are represented as mean ± SEM. (b, e) Two-tailed Mann Whitney *U* test.



## SUPPLEMENTARY INFORMATION

### Acute inhibition of transient receptor potential vanilloid-type 4 cation channel halts cytoskeletal dynamism in microglia.

Jolien Beeken, Melanie Mertens, Nathan Stas, Sofie Kessels, Liese Aerts, Bieke Janssen, Femke Mussen, Silvia Pinto, Rudi Vennekens, Jean-Michel Rigo, Laurent Nguyen, Bert Brône, Yeranddy A. Alpizar

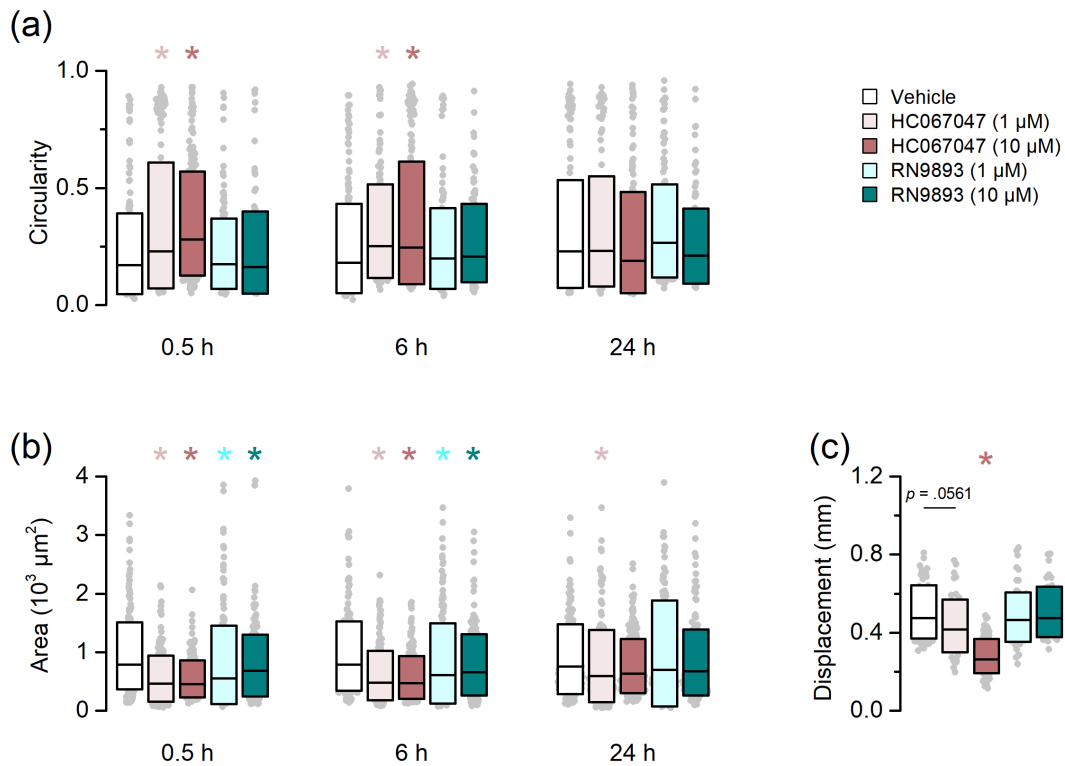


**Figure S1:** Differential effects of TRPV4 inhibitors on the morphological and migratory changes on wild type microglia *in vitro*. (a, b) Circularity and area parameters on wild type primary microglia after acute inhibition of TRPV4 with HC067047 and RN9893 ( $n \geq 202$  per condition). (c) Total displacement in 6 h during persistent random walk in the presence of TRPV4 inhibitors. ( $n \geq 62$  cells per condition). Asterisks indicate statistically significant differences (of at least  $p < .05$ ) with vehicle-treated cells (Vehicle, 0.2% DMSO); two-tailed Dunn's multiple comparison test.

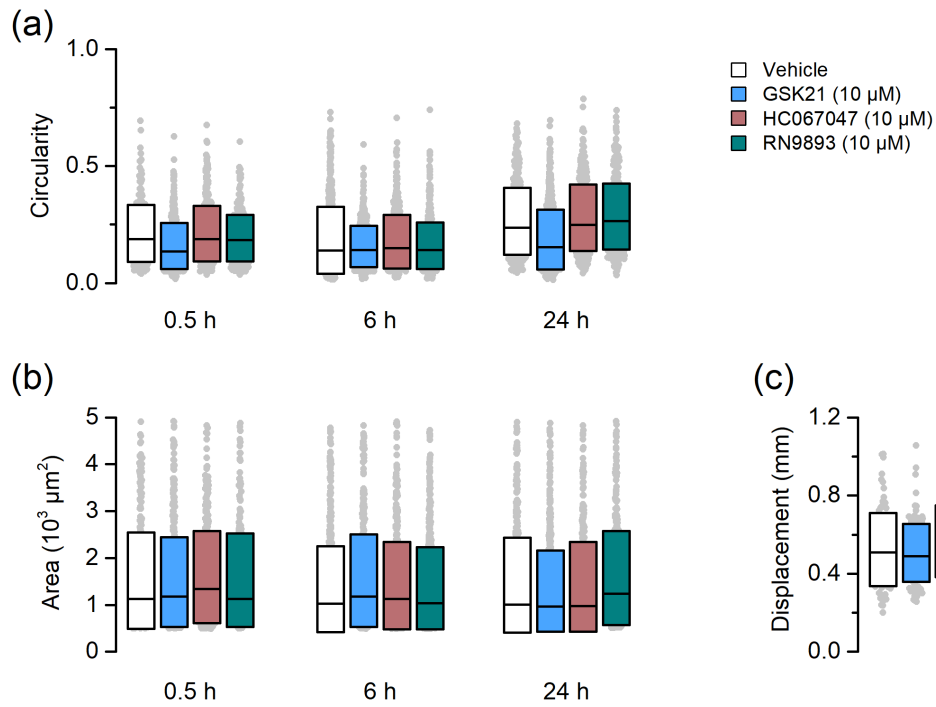


**Figure S2:** No off-target effects were induced by 3 different TRPV4 inhibitors on morphological and migratory parameters of TRPV4-deficient microglia *in vitro*. Statistical comparisons revealed no morphological differences compared to the vehicle-treated cells ( $n \geq 162$  per genotype, two-tailed Dunn's multiple comparison test). (c) Total displacement in 6 h during persistent random walk of *Trpv4* KO primary microglia treated with TRPV4 inhibitors. Two-tailed Dunn's multiple comparison test,  $n \geq 67$  cells per condition.

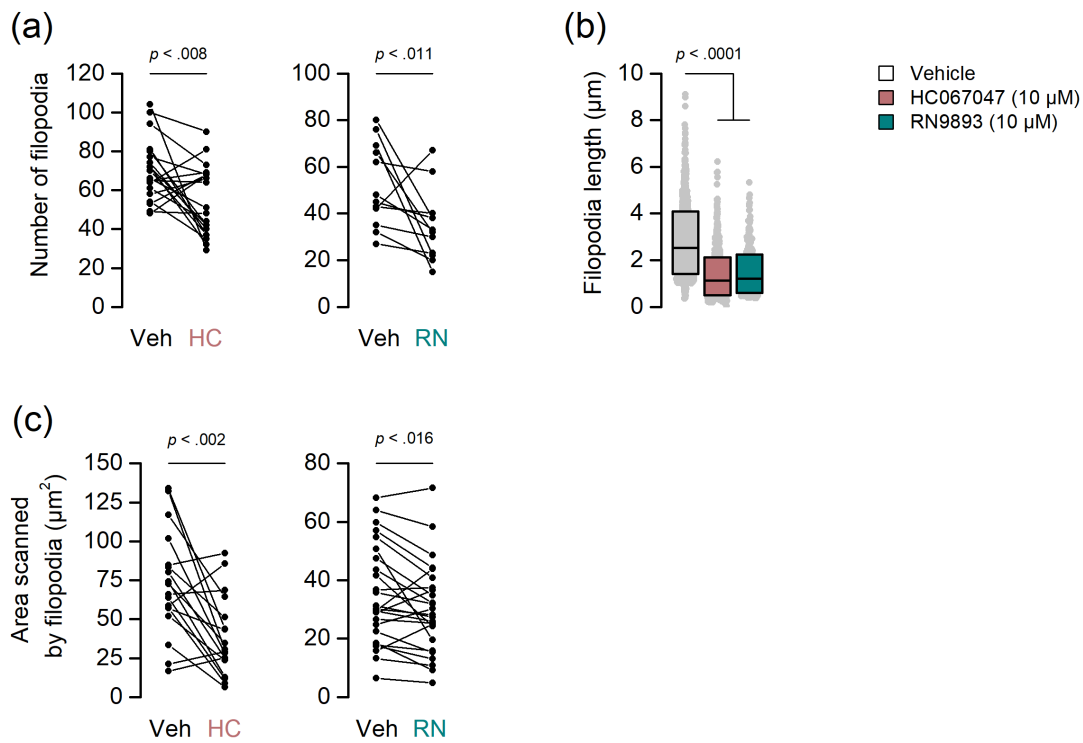


**Figure S3:** Acute inhibition of TRPV4 decreases length and motility of actin-rich filopodia in wild type microglia. (a) Number of filopodia during incubation with vehicle (0.2% DMSO) and after acute inhibition of TRPV4 (HC067047, RN9893). Data points represent individual regions ( $n_{HC} = 20$ ,  $n_{RN} = 12$ ) from 5 cells. Wilcoxon matched-pairs signed rank test. (b) Length of filopodia before (0.2% DMSO, Vehicle) and after acute inhibition of TRPV4. Data points represent individual filopodia ( $n \geq 416$  per condition). Two-tailed Mann Whitney  $U$  test. (c) Total scanned area by filopodia in selected regions ( $n_{HC} = 18$ ,  $n_{RN} = 25$ ; 8 cells). Wilcoxon matched-pairs signed rank test.

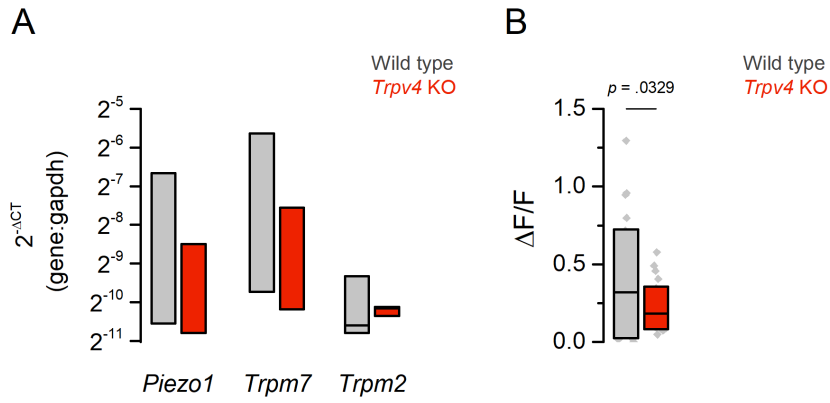


**Figure S4:** Expression profile of *Piezo1*, *Trpm7* and *Trpm2* in microglia of *Trpv4* KO mice. (a) Relative mRNA expression of *Piezo1*, *Trpm7* and *Trpm2* in wild type and *Trpv4* KO microglia. Boxes represent the median and SD of delta Ct values, normalized to *Gapdh* expression (n = 3 mice per genotype). (b) Maximum amplitudes of intracellular Ca<sup>2+</sup> levels in response to Yoda-1 (10 μM) recorded in wild type and *Trpv4* KO conditions. Boxes represent mean ± SD; Mann-Whitney U test.

**Table S1.**

*P* values for paired comparisons (Dunn's multiple comparison test) of data shown in Figure 1e.

	0.5 h			6 h			24 h			48 h			
	Ctrl	1 $\mu$ M	10 $\mu$ M	Ctrl	1 $\mu$ M	10 $\mu$ M	Ctrl	1 $\mu$ M	10 $\mu$ M	Ctrl	1 $\mu$ M	10 $\mu$ M	
Ctrl		0.0023	<0.0001		0.0098	<0.0001		<0.0001	<0.0001		<0.0001	<0.0001	Area
1 $\mu$ M	0.1720		<0.0001	0.2911		<0.0001	>0.9999		0.0010	<0.0001		>0.9999	
10 $\mu$ M	0.0001	<0.0001		<0.0001	<0.0001		<0.0001	<0.0001		<0.0001	<0.0001		
Circularity													

**Supplementary movie 1:** Representative video showing highly dynamic microtubules in WT microglia over a timespan of 2.5 min.

**Supplementary movie 2:** Acute inhibition of TRPV4 drastically decreases tubulin dynamics.

**Supplementary movie 3:** Filopodia movement before and after treatment with the TRPV4 antagonist.

## SUPPLEMENTARY METHODS

### *Quantitative real-time PCR*

RNA was isolated from freshly-isolated CD11b<sup>+</sup> cells extracted from WT and *Trpv4*<sup>-/-</sup> P21 brains using the RNeasy Mini Kit (Qiagen, Germany) following manufacturer's instructions. cDNA was synthesized through reverse transcription with the qScript cDNA SuperMix (VWR, Radnor, US) and diluted to a final concentration of 5 ng/μl. The cDNA was amplified by real-time PCR on the StepOnePlus Real-Time PCR system (Applied Biosystems, Foster City, US) using the SYBR Green Master Mix (Applied Biosystems), probes for *Piezo1*, *Piezo2*, *Trpm7*, *Trpm2* and *Gapdh*. *Piezo2* was not detected after 40 cycles, data not shown. Custom-made (*Trpm2*) or commercially available (*Piezo1*, *Piezo2*, *Trpm7*) primers were purchased at Integrated DNA Technologies (Leuven, Belgium).

*Trpm2* (fwd: 5'-ACAACCCTGAAGGACAGTGG-3'; rev: 5'-CATCACTAGCACCTCCAGCA-3')

*Trpm7* (Mm.PT.58.13777605)

*Piezo1* (Mm.PT.58.11048868)

*Piezo2* (Mm.PT.58.30174298)

### *Live-cell Ca<sup>2+</sup> imaging*

TIC medium-cultured, WT and *Trpv4* KO microglia seeded in MatTek glass bottom were incubated with Fluo-4 (2 μM, Invitrogen, USA) for 30 min. Afterwards, cells were rinsed and imaged before and after being exposed to solutions containing Yoda-1 (10 μM, Tocris Bioscience, Bristol, United Kingdom) prepared in Krebs (in mM: 150 NaCl, 6 KCl, 10 HEPES, 10 glucose, 1.5 CaCl<sub>2</sub>, 1 MgCl<sub>2</sub>, pH 7.4) either manually or via perfusion by gravity using a multi-barrelled pipette tip. Time-lapse live-cell Ca<sup>2+</sup> imaging was performed with Zeiss Elyra PS.1 widefield fluorescence microscope with a 488 nm excitation laser and a laser power of 1%. Images were captured at one frame per second using a PCO Edge 4.2 sCMOS camera connected with an Ander iXon+ 897 EMCCD camera at a magnification of 10x. Acquired images were processed with Fiji (ImageJ v2.0, Open source software). For each time point, the mean pixel intensity in the soma was calculated. The response amplitude was calculated and normalized by the average pixel intensity of the baseline.